A&A 471, 453–465 (2007)
DOI: 10.1051/0004-6361:20066967

Astronomy & Astrophysics

Resolving the innermost parsec of Centaurus A at mid-infrared wavelengths⋆

K. Meisenheimer[1], K. R. W. Tristram[1], W. Jaffe[2], F. Israel[2], N. Neumayer[1], D. Raban[2], H. Röttgering[2], W. D. Cotton[3], U. Graser[1], Th. Henning[1], Ch. Leinert[1], B. Lopez[4], G. Perrin[5], and A. Prieto[1]

[1] Max-Planck-Institut für Astronomie, Königstuhl 17, 69117 Heidelberg, Germany
e-mail: meisenheimer@mpia.de
[2] Sterrewacht Leiden, Niels-Bohr-Weg 2, 2300 CA Leiden, The Netherlands
[3] NRAO, 520 Edgemont Road, Charlottsville, VA 22903-2475, USA
[4] Observatoire de la Côte d'Azur, Boulevard de l'Observatoire, BP 4229, 06304 Nice Cedex 4, France
[5] Observatoire de Paris, LESIA, UMR 8109, 92190 Meudon, France

Received 19 December 2006 / Accepted 14 May 2007

ABSTRACT

Context. To reveal the origin of mid-infrared radiation from the core of Centaurus A, we carried out interferometric observations with the MID-infrared Interferometer (MIDI) at ESO's VLTI telescope array.
Aims. Observations were obtained with four baselines between unit telescopes of the VLTI, two of them roughly along the radio axis and two orthogonal to it. The interferometric measurements are spectrally resolved with $\lambda/\Delta\lambda = 30$ in the wavelength range 8 to 13 μm. Their resolution reaches 15 mas at the shortest wavelengths. Supplementary observations were obtained in the near-infrared with the adaptive optics instrument NACO, and at mm wavelengths with SEST and JCMT.
Methods. The mid-infrared emission from the core of Centaurus A is dominated by an unresolved point source (<10 mas). Observations with baselines orientated perpendicular to the radio jet reveal an extended component which can be interpreted as a geometrically thin, dusty disk, the axis of which is aligned with the radio jet. Its diameter is about 0.6 pc. It contributes between 20% (at $\lambda \simeq 8$ μm) and 40% (at $\lambda \simeq 13$ μm) to the nuclear flux from Centaurus A and contains dust at about 240 K. We argue, that the unresolved emission is dominated by a synchrotron source. Its overall spectrum is characterized by an $F_\nu \sim \nu^{-0.36}$ power-law which cuts off exponentially towards high frequencies at $\nu_c = 8 \times 10^{13}$ Hz and becomes optically thick at $\nu < \nu_1 \simeq 45$ GHz.
Results. Based on a Synchrotron Self Compton (SSC) interpretation for the γ-ray emission, we find a magnetic field strength of 26 μT and a maximum energy of relativistic electrons of $\gamma_c = E_c/m_e c^2 = 8500$. Near γ_c, the acceleration time scale is $\tau_{acc} = 4$ days, in good agreement with the fastest flux variations, observed at X-ray frequencies. Our SSC model argues for a Doppler factor $\delta \simeq 1$ which – together with the jet-counter jet ratio of the radio jets on parsec scale – results in an upper limit for the bulk Lorentz factor $\Gamma_{jet} < 2.5$, at variance with the concept of a "mis-directed BL Lac object".
Conclusions. We estimate a thermal luminosity of the core, $P_{th} \simeq 1.3 \times 10^{34}$ W $= 1.5 \times 10^{-4} \times L_{Edd}$, intermediate between the values for highly efficiently accreting AGN (e.g. Seyfert galaxies) and those of typical FR I radio galaxies. This luminosity, which is predominantly released in X-rays, is most likely generated in an Advection Dominated Accretion Flow (ADAF) and seems just sufficient to heat the dusty disk.

Key words. galaxies: individual: Centaurus A (NGC 5128) – galaxies: nuclei – radiation mechanism: non-thermal – techniques: interferometric – methods: observational

Centaurus A (NGC 5128) is the closest active galaxy. Its activity was first noticed at radio frequencies (Bolton et al. 1949) where it is one of the brightest and largest objects in the sky, extending over about $8° \times 3°$ (Junkes et al. 1993). An inner system of radio jets and lobes, about 12′ in size (Clarke et al. 1992) has also been detected in X-rays (Döbereiner et al. 1996; Hardcastle et al. 2003). The source of this large scale activity is an Active Galactic Nucleus (AGN) in the center of an elliptical galaxy, which is undergoing late stages of a merger event with a spiral galaxy (Baade & Minkowski 1954). The core of Centaurus A is heavily obscured by the dust lane of the spiral and becomes visible only at wavelengths longwards of 0.8 μm (Schreier et al. 1998; Marconi et al. 2000). It harbors a super-massive black hole, the mass of which has recently been determined from the velocity field in a circum-nuclear gas disk to be $M = 6 \times 10^7$ $M_\odot$ (Häring-Neumayer et al. 2006). See Israel (1998) for a comprehensive review of general properties of Centaurus A.

Centaurus A's close distance of only 3.84 Mpc (Rejkuba 2004)[1] offers unique opportunities to look into the very core of an AGN, as 1 parsec corresponds to 53 mas (milli-arcseconds). Despite this fact, single-telescope observations have not been able to resolve the core at any wavelength: at short wavelengths (~1 μm) the upper limit for its size is about 100 mas (1.9 pc). Radio interferometry with VLBI networks reveals a core – jet structure within the central parsec: the well-collimated radio jet can be traced over >60 mas at $\lambda = 6$ cm (Tingay et al. 1998). Also a counter-jet is clearly detected. Nevertheless, the radio core (with inverted spectrum $S_\nu \sim \nu^2$ between 6 and

⋆ Based on observations made with the Very Large Telescope Interferometer at the European Southern Observatory on Cerro Paranal.

[1] Recent distance measurement of Centaurus A range between 3.4 and 4.2 Mpc with typical uncertainties of ±10%.

Table 1. Log of the MIDI observations of Centaurus A and the calibrator HD 112213. The derived correlated flux (averaged over ±0.2 μm) is given for two wavelengths, least affected by the silicate absorption.

Date: Telescopes Target	LST	Baseline length	 PA	Resolution[a]	Correlated flux $\lambda = 8.3\,\mu$m	 $\lambda = 12.6\,\mu$m
	[h]	[m]	[degree]	[mas]	[Jy]	[Jy]
28-Feb.-2005: UT3–UT4						
Cen A	12:02	58.2	96	14.8	0.45 ± 0.04	0.73 ± 0.05
HD 112213	12:26	61.3	105	14.0		
Cen A	14.24	62.4	120	13.6	0.34 ± 0.05	0.60 ± 0.05
HD 112213	14:50	61.1	130	13.9		
26-May-2005: UT2–UT3						
Cen A	11:53	46.5	27	18.2	0.66 ± 0.04	0.91 ± 0.06
HD 112213	12:44	45.5	40	17.7		
Cen A	14:05	44.1	46	19.2	0.76 ± 0.04	1.01 ± 0.06
HD 112213	14:32	41.5	54	20.4		

[a] Resolution $\lambda/2B$ at $\lambda = 8.3\,\mu$m.

1 cm) is hardly resolved even with millimeter VLBI: at 43 GHz Kellermann et al. (1997) find an angular diameter (*FWHM*) of 0.5 ± 0.1 mas (0.01 pc).

The nature of the near- and mid-infrared emission from the parsec-size core of Centaurus A remains a matter of debate. Although several authors (e.g. Bailey et al. 1986; Turner et al. 1992; Chiaberge et al. 2001) have argued that high frequency synchrotron radiation might be an important contribution to the emission, others assume that the extremely red near-infrared colors of the unresolved core hint to the existence of a hot, AGN-heated dust structure (see Israel 1998, and references therein), which has been postulated to exist in the central parsec of more luminous AGN and has recently been resolved by mid-infrared interferometry of nearby Seyfert 2 galaxies (Jaffe et al. 2004; Ratzka et al. 2006; Tristram et al. 2006). In order to resolve the core emission on sub-parsec scales, interferometric observations are mandatory. In this paper we will report on the first high-frequency interferometry of Centaurus A, which was obtained with the Very Large Telescope Interferometer (VLTI) of the European Southern Observatory (ESO).

1. Observations

1.1. Interferometric observations with MIDI

The interferometric observations of Centaurus A were obtained with the MID-infrared Interferometric instrument (MIDI) at the Very Large Telescope Interferometer (VLTI) during two nights of guaranteed time on February 28 and May 26, 2005 (see log of the interferometric observations in Table 1). We used two telescope combinations with roughly orthogonal configuration: UT3–UT4 and UT2–UT3.

MIDI is a classical Michelson type stellar interferometer combining the beams of two 8 m unit telescopes (UTs) of the VLTI in the *N*-band. By insertion of a NaCl prism into the light path, the instrument produces spectrally dispersed fringes from 7.8 to 13.2 μm with a spectral resolution of $R \sim 30$ (Leinert et al. 2003; Morel et al. 2004). At both telescopes the wavefront was corrected using the adaptive optics system MACAO (Arsenault et al. 2003). We adopted the following observing procedure:

First, MIDI was used in imaging mode to center the object on the detector, thus ensuring an overlap of the two incoming beams for the interferometric measurement. Chopping of the UT secondaries removes the sky background (chopping frequency $f = 2$ Hz, position angle $\alpha = 0°$ and chopping throw $\delta = 15''$). Our experience is, that for weak targets this imaging is the most challenging part of the observation as background gradients hamper the detection of faint sources[2]. The short wave N band filter at 8.7 μm and an exposure time of 4 ms were used for the acquisition. To obtain a clear detection of the nucleus of Centaurus A a total of 3000 to 5000 exposures had to be taken.

For the interferometric observations the beam combiner, a $0.6'' \times 2''$ slit and the NaCl prism were inserted into the light path, resulting in two spectrally dispersed interferometric signals of opposite phase on the detector. Fringes were searched by scanning with the VLTI delay lines a few millimetres around the expected position of zero optical path difference (OPD) while MIDI's internal piezo-driven mirrors vary the OPD rapidly. No chopping is needed during interferometric measurements as the uncorrelated background signal can be removed with a software high-pass filter from the modulated fringe signal. After the fringe search had determined zero OPD, the integration in fringe tracking mode was started. In this mode the MIDI piezos change the OPD over 80 μm in order to estimate the position of zero OPD in real time from the fringe movement in every scan. For most fringe tracking observations the integration time per frame was `DIT` = 12 ms, which was increased to `DIT` = 18 ms for the second observation on May 26. We took `NDIT` = 8000 frames per fringe tracking on February 28, and `NDIT` = 5000 on May 26. We used the offset tracking mode, at an offset of 50 μm from zero OPD.

The interferometric integration was followed by two sequences of photometric data: With one shutter open, only the light from telescope A falls on the beam splitter producing two photometry signals on the detector. The integration time during photometry of Centaurus A was 12 ms, and the total number of photometry frames was increased from 4000 in the first measurement in February to 10 000 frames for the measurements in May. Again chopping had to be used for the photometric measurements. The same procedure was repeated with only the shutter of telescope B open.

After observing Centaurus A, the entire procedure: centering, fringe search, fringe track and photometry was repeated for the calibrator star HD 112213, to enable a correction for atmospheric transparency and instrumental visibility in the data reduction.

[2] This will improve with the introduction of Variable Curvature Mirrors (VCMs) which were not available during our observations.

1.2. Data reduction of interferometric observations

All interferometric and photometric data were reduced with the EWS package (version 1.3, see Jaffe 2004). For each set of measurements essentially two spectra, the raw *correlated flux* $C_{\rm corr}(\lambda)$ and the raw *total flux* $C_{\rm tot}(\lambda)$ (both measured in ADU counts/s), as well as the raw *visibility* $V^{\rm raw}(\lambda) \equiv C_{\rm corr}(\lambda)/C_{\rm tot}(\lambda)$ are determined and subsequently calibrated by using the measurements of the standard star.

To get $C_{\rm corr}(\lambda)$ the dispersed fringe signal is extracted using a spatial weighting function ("mask") which optimizes the signal-to-noise ratio. In order to sample the point spread function of our observations (0.″6 *FWHM*), we use a weighting function with an effective width of 0.″70. The two opposite phased signals are subtracted, thus removing residual background and doubling the signal amplitude. The individual data frames are phased to the same zero optical path difference (OPD) and averaged. Frames with largely discrepant OPD values are rejected.

The raw total flux $C_{\rm tot}(\lambda)$ is extracted from the photometric frames after subtracting the (chopped) background measurements. The same spatial mask as for the interferometric measurements is used. In order to correct for any residual background, the sky value is interpolated between two sky windows running above and below the object spectrum, respectively. For the observations of Centaurus A, the best sky subtraction[3] was obtained when using two sky windows located at 0.″39 to 0.″90 above and below the object spectrum, respectively. The raw total flux $C_{\rm tot}$ is calculated as $\sqrt{A_1 \cdot B_1} + \sqrt{A_2 \cdot B_2}$ with A_1 the photometry of beam A (from the first telescope) in channel 1, B_1 the photometry of beam B (from the second telescope) in channel 1, as well as A_2 and B_2 the corresponding beams in channel 2. So defined, $C_{\rm tot}$ equals the value of $C_{\rm corr}$ that would be expected from the same telescopes/instrument system for a *point source*.

The *raw visibility*, calculated as $V^{\rm raw}(\lambda) \equiv C_{\rm corr}(\lambda)/C_{\rm tot}(\lambda)$ is relatively insensitive to differences in atmospheric seeing between target and calibrator observations and is commonly used as the principal output of an interferometer. However it is very sensitive to photometric errors caused by background fluctuations, which are important in the mid infrared, and in some cases the direct interpretation of $C_{\rm corr}$ is preferable. These issues will be discussed in detail in Sect. 2.

To calculate the total flux $F_{\rm tot}$ displayed in Fig. 1, we use a slightly different raw total flux $C'_{\rm tot}(\lambda)$ which is determined as $C_{\rm tot}(\lambda)$ but by averaging the four measurements linearly and *without* applying the mask: $C'_{\rm tot} = \frac{1}{4}(A_1 + B_1 + A_2 + B_2)$. While not appropriate for calculating visibilities, this definition of $C'_{\rm tot}$ is less sensitive to changes in telescope pointing and atmospheric seeing than $C_{\rm tot}$ and thus more useful for estimating variations in the total flux of Centaurus A.

For the standard star of known flux and visibility, the same reduction steps lead to raw fluxes $C^*_{\rm corr}(\lambda)$, $C^*_{\rm tot}(\lambda)$, $C'^*_{\rm tot}(\lambda)$, and the raw visibility $V^{*,\rm raw}(\lambda)$. The *calibrated* flux densities[4] (in Jy) of Centaurus A are then derived from the known flux $F^*(\lambda)$ of HD 112213 (spectrum based on template fit to five band photometry, van Boekel, priv. comm.) according to:

correlated flux density	$F_{\rm corr}(\lambda) = C_{\rm corr}(\lambda) \cdot [F^*(\lambda)/C^*_{\rm corr}(\lambda)]$,
total flux density	$F_{\rm tot}(\lambda) = C'_{\rm tot}(\lambda) \cdot [F^*(\lambda)/C'^*_{\rm tot}(\lambda)]$,

[3] That is, the most consistent $C_{\rm tot}(\lambda)$ for all four independent measurements.

[4] In the following, we will abbreviate these flux densities as total and correlated *flux*, respectively.

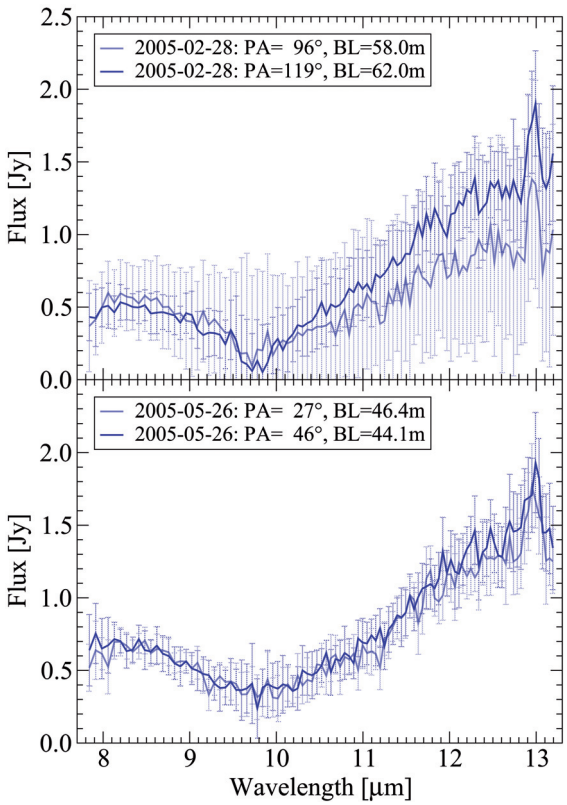

Fig. 1. Spectrum of the total flux $F_{\rm tot}$ between 8 and 13 μm as observed on February 28 (*top panel*) and on May 26, 2005 (*bottom panel*). The obvious differences in $F_{\rm tot}$ are caused by imperfect background subtraction (see text). The errors are dominated by systematic uncertainties. Note the broad silicate absorption feature at $8.5 < \lambda < 12\,\mu$m and the [NeII] emission line at $\lambda = 12.90\,\mu$m.

The calibrated *visibility* as a function of wavelength, is derived by: $V(\lambda) = 1 \cdot [V^{\rm raw}(\lambda)/V^{\rm raw,*}(\lambda)]$, where HD 112213 (diameter: 2.95 mas) is assumed to be point-like ($V^*(\lambda) \equiv 1$).

1.3. Additional single-telescope observations

1.3.1. Near-infrared photometry at $1.2 < \lambda < 2.2\,\mu$m with NACO

Near-infrared observations were performed on June 12 and 14, 2003, and on April 1, 2004 with Naos-Conica (NACO) at UT4. NACO consists of the high-resolution near-infrared imager and spectrograph Conica (Lenzen et al. 1998) and the Nasmyth Adaptive Optics System (Naos) (Rousset et al. 1998). It provides adaptive-optics corrected observations in the range of 1–5 μm with 14″ to 54″ fields of view and 13 to 54 mas pixel scales. The data were taken in visitor mode and seeing during observations was in the range 0.″3–0.″8 (as measured by the seeing monitor in V-band), with clear/photometric conditions.

There are no potential reference stars bright enough ($m_K \leq$ 14 mag) for the wavefront correction at a distance of ≤30″ to the nucleus, necessary for a good quality of correction at the nucleus. Therefore, we directly guided on the nucleus itself using the unique IR wavefront sensor (WFS) implemented in Naos. This strategy provides us the best possible wavefront correction in the vicinity of the active galactic nucleus (AGN). During the observations the atmospheric conditions were stable and the performance of the IR WFS was continually very good. For observations in J-band we used the K-dichroic, i.e. all the nuclear

Table 2. Flux measurement of the core of Centaurus A.

Frequency [Hz]	Wavelength [μm]	F_ν [Jy]	$F_{\nu,0}$[a] [Jy]	Date[b] [year]	Instrument	Beamwidth [mas]	Reference
4.8×10^9	63 000	1.2		1993.13	VLBI	2.6	Tingay et al. (1998)
8.4×10^9	35 700	2.4		1996.22	VLBA	2.4	Tingay et al. (1998)
22.2×10^9	13 500	3.5		1995.88	VLBA	1.2	Tingay et al. (1998)
90.0×10^9	3530	8.6 ± 0.6		2003.18	SEST	57 000	this paper
1.50×10^{11}	2000	6.9 ± 0.3		2003.18	SEST	32 000	this paper
2.35×10^{11}	1270	5.8 ± 0.2		2003.18	SEST	20 000	this paper
2.70×10^{11}	1110	5.9 ± 1.0		2003.30	JCMT	18 000	this paper
3.75×10^{11}	800	8.5		1991.35	JCMT	14 000	Hawarden et al. (1993)
6.67×10^{11}	450	6.3		1991.35	JCMT	10 000	Hawarden et al. (1993)
2.38×10^{13}	12.6	0.62 ± 0.03	1.125	2005.28	MIDI	22	this paper
2.63×10^{13}	11.4	0.43 ± 0.03	1.074	2005.28	MIDI	20	this paper
2.88×10^{13}	10.4	0.25 ± 0.02	0.987	2005.28	MIDI	17	this paper
3.23×10^{13}	9.3	0.28 ± 0.02	1.135	2005.28	MIDI	17	this paper
3.61×10^{13}	8.3	0.47 ± 0.05	0.869	2005.28	MIDI	14	this paper
7.90×10^{13}	3.80	0.20 ± 0.04	0.368	2003.36	NACO	90	Prieto, priv. comm.
1.35×10^{14}	2.22	41.5×10^{-3}	0.190	1997.61	NICMOS	250	Marconi et al. (2000)
1.39×10^{14}	2.15	$(33.7 \pm 2.0) \times 10^{-3}$	0.169	2004.25	NACO	59	this paper
1.80×10^{14}	1.67	$(4.5 \pm 0.3) \times 10^{-3}$	0.052	2003.45	NACO	88	this paper
1.87×10^{14}	1.60	4.8×10^{-3}	0.065	1997.69	NICMOS	170	Marconi et al. (2000)
2.34×10^{14}	1.28	$(1.3 \pm 0.1) \times 10^{-3}$	0.049	2003.45	NACO	100	this paper
3.69×10^{14}	0.81	7×10^{-6}	0.010	1997.80	WFPC2	100	Marconi et al. (2000)

[a] Corrected for extinction by adopting $A_V = 14$ mag (see text).
[b] In cases in which several observations were averaged, we give an average date.

K-band light was used for the wavefront correction. While observing in K-band itself the only possibility to achieve a good performance of the WFS was to send 90% of the light to NAOS and only 10% to Conica (i.e. to use the N90C10 dichroic). In H-band we also used the N90C10 dichroic, to get the best possible correction.

To remove bad pixels and cosmics we jittered the field on several positions on the detector. The on-chip exposure time was 60 s in J-, 20 s in H-, and 120 s K-band and the total exposure time 20 min in J-band, 13 min in H-, and 40 min in K-band.

For the flux calibration a separate PSF star was observed directly before and after the nucleus of Centaurus A with the same WFS setup and exposure time. This star was chosen from the 2MASS point source catalogue (Cutri et al. 2003) to match Centaurus A's nucleus as closely as possible in angular proximity, magnitude and color.

The nucleus is unresolved at all wavelengths with a size (*FWHM*) of 0.″10 in J-, 0.″088 in H-, and 0.″059 in K-band. The flux values given in Table 2 are extracted in circular apertures of 0.″20, 0.″18, and 0.″12 diameter in J, H and K, respectively (for details refer to Neumayer et al., in preparation).

1.3.2. Millimeter observations with the SEST and the JCMT

We determined flux densities of the Centaurus A nucleus in the millimeter wavelength range with the 15 m Swedish-ESO Submillimetre Telescope (SEST) on Cerro La Silla (Chile). The measurements presented here were obtained in February and March 2003 as close in time as possible to the epoch of the MIDI and NACO observations discussed in this paper.

The SEST beamsize ranges from 57″ at 85 GHz to 14″ at 345 GHz. Using scans we have determined that, at least up to 230 GHz, the continuum source is unresolved by these beams. The SEST measurements were made with a chopping secondary in double-beamswitching mode, with a throw of 11′. Because the primary aim of the observations was a study of the absorption-line spectrum of Centaurus A, a special effort was made to get a well-defined continuum level by frequent pointing and calibration. Moreover, seen from Chile, the galaxy culminates at very small zenith angles. For these reasons, the SEST measurements of the unresolved continuum nucleus are quite accurate, as is also indicated by the small dispersion (less than 5%) of individual measurements in the 3 mm and 2 mm windows. At higher frequencies (and shorter wavelengths of 1.3 mm and 0.9 mm), both the smaller beam (making pointing more critical) and a poorer sky transmission cause the accuracy to be somewhat worse (typically about 15−20%). The continuum levels were measured in each individual spectrum in the velocity intervals 0−300 km s^{-1} and 800−1100 km s^{-1} (local standard of rest), well clear of molecular line emission centering on a systemic velocity of about 550 km s^{-1}. We have used these data to construct a best fit millimeter spectrum (frequency range 85−270 GHz) with spectral index ($S_\nu \sim \nu^\alpha$) $\alpha = -0.41 \pm 0.05$, and extracted for each receiver band the standardized flux densities at 90, 150 and 230 GHz listed in Table 2.

In March, May and July 2003, we also obtained measurements at 265/268 GHz with the 15 m James Clerk Maxwell Telescope (JCMT) on Mauna Kea (Hawaii), the mean of which is also listed in Table 2. The JCMT beam at these frequencies was about 18″. From Hawaii, Centaurus A never rises very high in the sky, and is in fact observable only during a few hours per day. Moreover, the observations were made in single-beamswitch only, with a throw of 3′. The JCMT observations are therefore less accurate (dispersion between individual scans about 20%). In addition, we measured the nuclear flux-density in the 0.85 mm window (330/345 GHz) a number of times in the same period during which the MIDI and NACO observations were made (2003.30−2005.25). Over the full two-year period, these JCMT measurements suggest a significant drop in nuclear

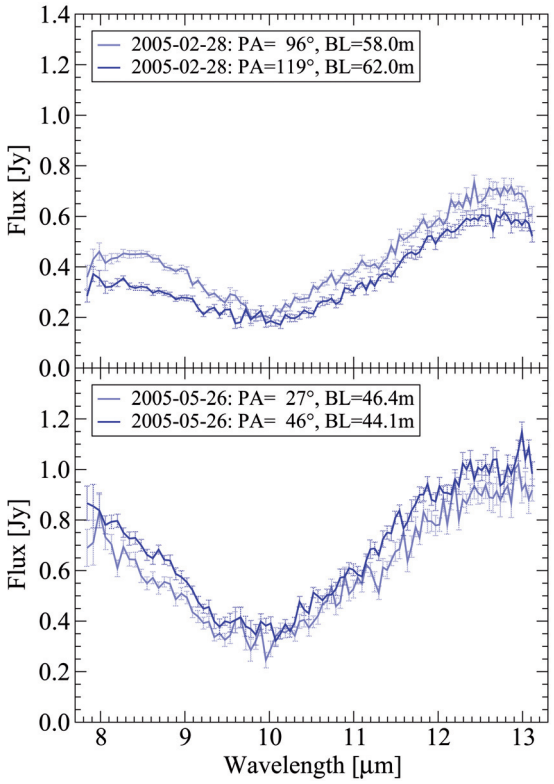

Fig. 2. Spectrum of the correlated flux $F_{\rm corr}$ between 8 and 13 μm as observed on February 28 (*top panel*) and on May 26, 2005 (*bottom panel*). Wavelengths $9.5 < \lambda < 10.1\,\mu$m are affected by the atmospheric ozone band. As for $F_{\rm tot}$ (Fig. 1) the spectral shape is dominated by silicate absorption, but no evidence for the [NeII] emission line is present. In contrast to Fig. 1, here the errors are dominated by photon noise.

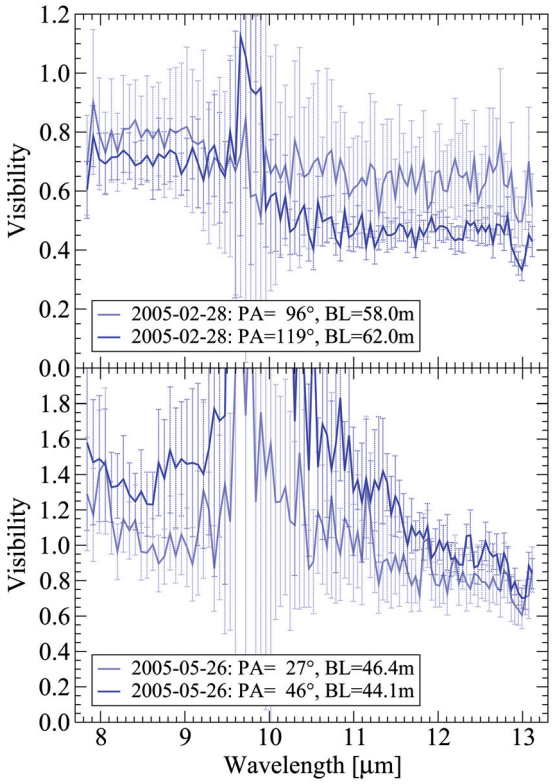

Fig. 3. Spectrum of the visibility $F_{\rm corr}/F_{\rm tot}$ between 8 and 13 μm as observed on February 28 (*top panel*) and on May 26, 2005 (*bottom panel*). Wavelengths $9.5 < \lambda < 10.1\,\mu$m are strongly affected by the atmospheric ozone band. Errors are dominated by the (systematic) errors in $F_{\rm tot}$.

intensity from about 7 Jy to 4.5 Jy (for more details see Israel et al., in preparation).

2. MIDI results

The results of our MIDI observations are summarized in Figs. 1 to 3 which show the *total* flux $F_{\rm tot}(\lambda)$, the *correlated* flux $F_{\rm corr}(\lambda)$, and the *visibility* $V(\lambda)$ between 8 and 13 μm as observed on February 28 and on May 26, 2005. Most of the observed spectral region is affected by the very broad absorption band due to silicates. The depth of the silicate feature is identical in $F_{\rm corr}$ and $F_{\rm tot}$, indicating that both the core and extended components suffer the same extinction. The [NeII] emission line at $\lambda = 12.90\,\mu$m is clearly detected in all four spectra displayed in Fig. 1, but not present in any of the correlated flux spectra in Fig. 2 which have superior signal-to-noise ratio. This indicates that the [NeII] emission line arises in an extended region (>50 mas), which is over-resolved by the interferometric observations.

Centaurus A was one of the first targets to be observed with MIDI with an average N-band flux $\langle F_{\rm tot}\rangle$ below 1 Jy. For such faint sources it is a greater challenge to measure the total flux $F_{\rm tot}$ accurately, rather than to determine the correlated flux, as the strong background naturally cancels out in the interferometric observations. Although Fig. 1 shows that we managed to get largely consistent results for $F_{\rm tot}$ in the two epochs, a closer inspection reveals discrepancies of 30% around 12 μm during one night (top panel: February 28). When comparing both nights we find deviations >35% in the silicate absorption feature (compare top and bottom panel) which can increase to more than a factor of 3 in the atmospheric ozone absorption band between 9.5 and 10.0 μm. We attribute these discrepancies to uncertainties in the background subtraction.

An estimate of the uncertainties in determining the correlated flux $F_{\rm corr}$ (see Fig. 2) might be obtained by comparing the measurements over one night (i.e. with similar baseline, see Table 1). Over most of the spectral range they are confined to ±10%. However, the significant difference between the measurements of $F_{\rm corr}$ on February 28 and on May 26 have to be interpreted as true interferometric signal, showing that the core of Centaurus A is marginally resolved along PA $\simeq 120°$ with a 60 m baseline.

Due to the afore mentioned uncertainties in $F_{\rm tot}$ it is hard to judge which of the details observed in the spectral visibilities $V(\lambda) = F_{\rm corr}/F_{\rm tot}$ displayed in Fig. 3 are real: clearly the values $V(\lambda) > 1$ obtained from the May 26 observations (lower panel) are caused by incorrect background subtraction in $F_{\rm tot}$ and thus indicate that the level of uncertainty in the visiblity measurements can reach 30%. Accordingly, we regard the two visibility measurements of February 28 (top panel) as consistent with each other despite the change in baseline position angle by 23°.

Taking all discussed uncertainties into account we conclude that there is no indication for intrinsic flux variability between the two observed epochs and that the most robust result of our measurements is the difference in correlated flux between the two observations (that is projected baselines). The ratio

$$f_{12} \equiv \frac{F_{\rm corr}(\text{Feb. 28})}{F_{\rm corr}(\text{May 26})}$$

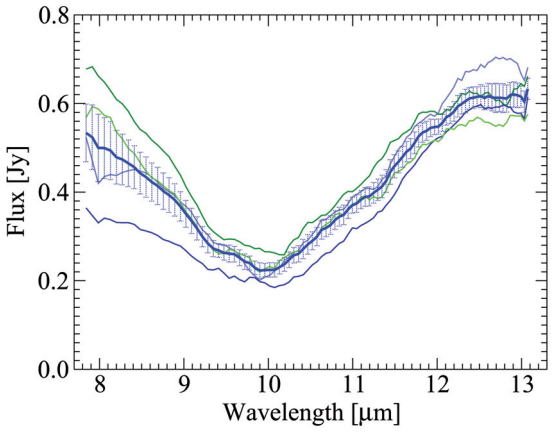

Fig. 4. Spectrum of the four individual measurements and the averaged correlated flux $F_{\rm corr}$ of the unresolved core (see text for details). The errors are derived from the scatter between the individual spectra.

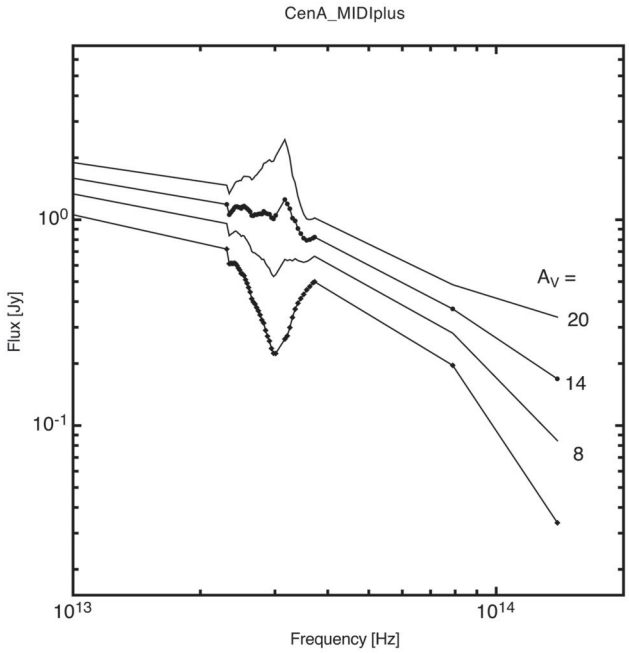

Fig. 5. Spectrum of the core of Centaurus A between 10^{13} and 2×10^{14} Hz for different value of the assumed foreground extinction. Filled diamonds show observed flux $F_{\rm corr}$ (averaged over all measurements), filled dots are corrected for the foreground extinction of $A_{\rm V} = 14$ mag. Remaining residuals of ±10% at $9.5\,\mu{\rm m} > \lambda > 8.2\,\mu{\rm m}$ are caused by an imperfect match of the short wavelength shape of the silicate absorption. Neither the assumption of minimum foreground extinction $A_{\rm V} = 8$ mag nor that of higher extinction $A_{\rm V} = 20$ mag does lead to a satisfactory removal of the silicate feature.

can be approximated by a linear function $f_{12}(\lambda) = 0.8{-}0.04\,(\lambda - 8\,\mu{\rm m})$ between 8 and 13 μm (compare Fig. 4). As on May 26 we find $F_{\rm corr} \equiv F_{\rm tot}$ within the errors, we regard $V^{\rm May\ 26}(\lambda) \simeq 1$ and $V^{\rm Feb.\ 28}(\lambda) = f_{12}(\lambda)$ as best measurements of the visibilities. The decrease in visibility towards longer wavelengths indicates that the source is significantly extended along PA $\simeq 120°$ and the extended emission has a spectrum which rises steeply between 9 and 13 μm, as expected for emission from thermal dust at temperatures $T < 300$ K (see detailed discussion in 4.2). We derive the spectrum of the compact core (Fig. 4) by averaging $F_{\rm corr}$(Feb. 28) and $f_{12}F_{\rm corr}$(May 26). From the formal 2σ-limit of the visibility around $\lambda = 8\,\mu$m observed on May 26 ($V \geq 0.9$), one derives an upper limit of about 6 mas *FWHM* for the size of the core.

3. The overall core spectrum of Centaurus A

In order to understand the nature of the – unresolved – core emission between 8 and 13 μm ($\nu = 2.3 \ldots 3.7 \times 10^{13}$ Hz) it is necessary to consider not only our interferometric measurements with MIDI but also our photometry at lower and higher frequencies, as well as supplementary data from the literature. At radio frequencies ($\nu < 43$ GHz, $\lambda > 7$ mm), this is straightforward as the VLBA clearly outperforms our mid-infrared interferometry in terms of resolution, and extinction is not an issue. Table 2 lists interferometric measurements of the core flux based on the VLBI and VLBA maps by Tingay et al. (1998). The spectrum of the radio core is strongly inverted, $\alpha \gtrsim 2$ for $F_\nu \sim \nu^\alpha$ (compare Fig. 6). It is unresolved at $\nu \leq 22$ GHz but has been marginally resolved at 43 GHz (0.5 ± 0.1 mas *FWHM*; Kellermann et al. 1997).

To determine the core spectrum in the (sub-)mm regime between 90 and 670 GHz (3 mm $> \lambda >$ 0.45 mm) is much more problematic due to the lack of interferometric data and the contribution of thermal emission of cold dust in the dust lane ($T \simeq 35$ K) shortwards of $\lambda \simeq 800\,\mu$m (Hawarden et al. 1993). Nevertheless, we think that our new millimeter photometry between 90 and 270 GHz – albeit obtained with single dish telescopes – should represent the core flux rather well, since the most important contaminants, the kiloparsec radio jet with its steep spectrum $F_\nu \sim \nu^{-0.75}$ (Clarke et al. 1992), and the thermal dust emission, dominant at shorter wavelengths, should be negligible here[5]. Indeed we find no deviations of our flux measurements between 90 and 270 GHz from a straight, non-thermal power-law $F_\nu \sim \nu^{-0.41}$. However, as illustrated by comparison of our photometry from 2003 with that derived 12 years earlier by Hawarden et al. (1993) from mapping observations at 800 and 450 μm (see Table 2 and Fig. 6) variability is significant at these wavelengths and can reach a factor of 1.5 or more. Thus one has to be careful when trying to reconstruct an overall spectrum from non-simultanous observations.

So far we have considered only radio to sub-mm frequencies, at which dust *extinction* can be neglected. This simplification certainly does not apply at $\lambda < 30\,\mu$m (10^{13} Hz): there is no way to obtain the intrinsic spectrum of the core of Centaurus A without correcting for the obvious extinction on our line-of-sight.

An absolute minimum for the extinction towards the core of Centaurus A is set by the value $A_{\rm V} \simeq 8$ mag determined from the arcsec-scale extinction map by Marconi et al. (2000) and Neumayer (priv. comm.). Presumably this extinction is caused by the dust lane in Centaurus A. However, based on the presence of a circum-nuclear disk of about 80 pc diameter, observed in molecular (Israel 1998) and ionized gas (Schreier et al. 1998; Marconi et al. 2000), it is expected that the total extinction on our line-of-sight towards the core is much higher. In fact, extinction values between $A_{\rm V} \simeq 14$ mag and $A_{\rm V} > 40$ mag have been discussed in the literature. Here we estimate the extinction towards the mid-infrared core by (i) assuming a galactic extinction law (Schartmann et al. 2005) with modified silicate profile (using Kemper et al. 2004), and (ii) requiring the extinction

[5] From Fig. 3 in Hawarden et al. (1993), we estimate a maximum contamination from the dust lane of <0.4 Jy (<10%) within our 18″ beam at 270 GHz.

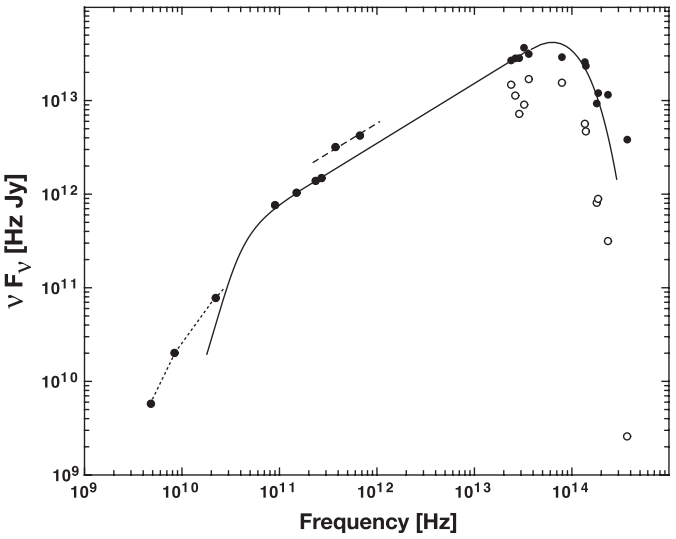

Fig. 6. Overall spectrum of the core of Centaurus A. Open circles show observed flux values, filled dots are corrected for the foreground extinction of $A_V = 14$ mag (compare Fig. 5). The synchrotron spectrum (solid line) shows an optically thin power-law $F_\nu \sim \nu^{-0.36}$ which cuts off exponentially at $\nu_c = 8 \times 10^{13}$ Hz, and is self-absorbed below $\nu_1 \simeq 4.5 \times 10^{10}$ Hz. Evidence for variability exists around 3×10^{11} Hz (dashed line through photometry in 1991) and above ν_c (various epochs between 1997 and 2005, cf. Table 2). The excess at cm wavelengths ($\nu < 2 \times 10^{10}$ Hz, connected by dotted lines) is due to optical thick components of larger size.

corrected spectrum in the range $8\,\mu\text{m} < \lambda < 13\,\mu\text{m}$ to be as smooth as possible, i.e. the prominent silicate feature disappears (see Fig. 5). This leads to our "best-guess" value $A_V = (14 \pm 2)$ mag, where the error is estimated from the fact that $A_V = 8$ mag and $A_V = 20$ mag are clearly rejected. Note that both our interpretation of the overall core spectrum at $\lambda < 1$ mm as optically thin synchrotron emission (see below) and the assumption of circum-nuclear dust emission virtually exclude values $A_V > 25$ mag since such high values would result in an erratic upturn of the intrinsic spectrum shortwards of 3 μm.

We list both the *observed* (F_ν) and *extinction corrected* ($F_{\nu,0}$) values of the core flux in Table 2, and display them in Fig. 6 as open circles and filled dots, respectively. The five values derived from our interferometric observations represent $F_{\rm corr}$ averaged over the measurement on February 28 and May 26, 2005. The solid line in Fig. 6 gives the best-fit standard synchrotron spectrum between 4×10^{10} and 2×10^{14} Hz. It is characterized by an optically thin power-law $F_\nu \sim \nu^{-0.36}$ which cuts off exponentially above some cutoff frequency $\nu_c = 8 \times 10^{13}$ Hz, and becomes optically thick below $\nu_1 = (45 \pm 5)$ GHz. We regard obvious discrepancies between this synchrotron spectrum, and the intrinsic, extinction corrected flux values $F_{\nu,0}$ as further evidence for variability of the core of Centaurus A. It should be noted, that for a synchrotron spectrum with high frequency cutoff one naturally expects high variability at $\nu \gtrsim \nu_c$ since small variations in ν_c can result in large flux variations. Indeed, variations by more than a factor 3 have been observed at 3.6 μm by Lepine et al. (1984) and at 3.3 μm by Turner et al. (1992).

4. Discussion

Our interferometric MIDI observations reveal the existence of two components in the inner parsec of Centaurus A: a resolved component, the "disk", which is most extended along PA $\simeq 120°$ and the unresolved "core". In Fig. 6 we demonstrate that the core spectrum can be fitted by a synchrotron spectrum with millimeter-to-mid-infrared power-law $F_\nu \sim \nu^{-0.36}$ which cuts off exponentially towards higher frequencies. However, the spatial resolution of our present observations is not sufficient to establish unambiguously the non-thermal nature of the core emission by a surface brightness argument. Before proceeding further with this interpretation, therefore, it is worthwhile to consider other explanations.

Marconi et al. (2000) have proposed an alternative model of the near-infrared spectrum of Centaurus A, which consists of a compact, hot black body (dust at $T = 700$ K) plus a non-thermal power-law $\sim\nu^{-0.9}$ which they had extrapolated from X-ray observations (Rothschild et al. 1999) to lower frequencies. In order to fit the spectrum, they had to assume that only the power-law component is reddened by $A_V \simeq 14$ mag, while the hot dust suffers no more than the foreground extinction ($A_V = 7.8$ mag). Furthermore, they argue that the hot blackbody could be small enough to show the observed 3.6 μm variability. There exist several problems with this model: first, our interferometric measurements prove that any core emission suffers at least $A_V = 14$ mag of extinction. Second, the steep X-ray spectrum $\sim\nu^{-0.9}$ has not been confirmed by subsequent observations with XMM and Chandra (Evans et al. 2004). The extrapolation of the true X-ray spectrum leads to a negligible contribution in the near-infrared. Also it should be noted, that exponential cut-offs are natural in synchrotron spectra and therefore no additional component is needed to explain the steep NIR spectrum of the core. Last but not least, both the variability at $\lambda \leq 3.6\,\mu$m which seems to be correlated with radio variations (Lepine et al. 1984, see also Fig. 6) and the high polarization (Bailey et al. 1986) are explained much more naturally in terms of a synchrotron model.

Therefore, we conclude that the core emission is dominated by non-thermal synchrotron radiation. On the other hand, the "disk" emission is most naturally explained by thermal emission of AGN heated dust at $T \simeq 300$ K as seen in other AGN. Further MIDI observations with projected baseline >100 m (using UT1−UT4) will allow us to pin down the flux ratio between "core" and "disk" more accurately. We defer a detailed discussion of the dust emission to Sect. 4.2 and start here with the discussion of the core spectrum.

The overall spectrum of the core in Centaurus A in Fig. 6 is reminiscent of millimeter-to-optical blazar spectra (see, e.g., Bregman 1990). This and the detection of γ-rays from Centaurus A has led several authors to jump on the conclusion that the core spectrum provides additional evidence for Centaurus A being a "mis-directed BL Lac object" (Bailey et al. 1986; Chiaberge et al. 2001). We do not want to follow this path for two reasons:

1. In the standard unified picture of BL Lac objects (Urry & Padovani 1995) normal FR I radio galaxies are the (misdirected) parent population of highly beamed BL Lac objects. Typical FR I cores are weak and their spectra normally do not extend beyond 10^{11} Hz.
2. With an optically thin $F_\nu \sim \nu^{-0.36}$ spectrum in the range between 10^{11} and 3×10^{13} Hz, the core spectrum of Centaurus A is exceptionally flat. Most classical blazars display much steeper spectra in this frequency range ($\alpha = -0.6 \ldots -0.9$)[6].

[6] It should be noticed, however, that the exceptionally flat spectrum of Centaurus A between 10^{11} and 3×10^{13} Hz is not unique: the nearby BL Lac object Mkn 421 also exhibits $\alpha \simeq -0.35$ in the same frequency range (Macomb et al. 1995).

4.1. The synchrotron core

The intrinsic properties of the core synchrotron source can be derived from observed properties and standard synchrotron theory (Pacholczyk 1970), in which the self-absorption frequency ν_1 and the synchrotron luminosity P_ν can be used to disentangle the strength of the magnetic field B and the number density of relativistic particles in a source of known size. In the following, we will first derive the basic properties of the synchrotron source in Centaurus A (in 4.1.1), and second discuss its relation to the radio jet (in 4.1.2).

4.1.1. Basic properties

The observed properties of the synchrotron core in Centaurus A are:

(a) The size determined by the VLBA observations at 43 GHz (Kellermann et al. 1997): taking their observed $FWHM$ = 0.5 mas = 0.0094 pc = 2.9×10^{14} m as diameter of a quasi-homogeneous blob, one derives a radius $R_{43} = 1.5 \times 10^{14}$ m for the synchrotron core. Comparing this with the Schwarzschild radius of the $M = 6 \times 10^7\, M_\odot$ black hole ($R_s = 1.8 \times 10^{11}$ m = 1.2 AU), one finds $R_{43} = 830\, R_s$.

(b) The slope of the optically thin synchrotron emission $F_\nu \sim \nu^\alpha$ with $\alpha = -0.36 \pm 0.01$ corresponds to an underlying electron energy distribution

$$n(\gamma)\mathrm{d}\gamma \equiv n_{1000}\left(\frac{\gamma}{1000}\right)^{-q}\mathrm{d}\gamma$$

(where we use $\gamma \equiv E/m_e c^2$ as dimensionless electron energy) with $q = 1 - 2\alpha = 1.72$.

Following standard synchrotron theory one can use a combination of

(c) the *intrinsic*[7] self-absorption frequency $\nu_1 \equiv \nu_{\tau=1} = (4.5 \pm 0.5) \times 10^{10}\, \delta^{-1}$ Hz, where $\delta = \sqrt{1-\beta_{\rm jet}^2}/(1-\beta_{\rm jet}\cos\theta)]$ is the Doppler factor of the emitting source moving with $\beta_{\rm jet} = v_{\rm jet}/c$ under an angle θ with respect to the line-of-sight, and the simplification

$$\tau = \int_0^R \kappa_\nu \mathrm{d}l \simeq \kappa_\nu R = 1, \quad \text{and}$$

(d) the emitted power at some (optically thin) frequency ν:

$$\begin{aligned} P_\nu(3\times10^{11}\,\mathrm{Hz}) &= 5.4\times10^{-26}\,\delta^{\alpha-2} 4\pi D_L^2 \ \ \mathrm{W\,Hz^{-1}} \\ &= 9.53\times10^{21}\delta^{\alpha-2} \ \ \mathrm{W\,Hz^{-1}}, \end{aligned}$$

to solve for the average magnetic field $\langle B\rangle$ and n_{1000}, respectively, since:

$$\kappa_\nu = \frac{1}{R} = c_\kappa(q)\cdot n_{1000}\left(\frac{\langle B\rangle}{1\,\mathrm{mT}}\right)^{1+q/2}\left(\frac{\nu_1}{\nu_0}\right)^{-2-q/2} \quad (1)$$

and

$$\epsilon_\nu = \frac{P_\nu}{\frac{4}{3}\pi R^3} = c_\epsilon(q)\cdot n_{1000}\left(\frac{\langle B\rangle}{1\,\mathrm{mT}}\right)^{1/2+q/2}\left(\frac{\nu_1}{\nu_0}\right)^{1/2-q/2}. \quad (2)$$

[7] Intrinsic values refer to the restframe of the synchrotron emitting source.

Here we assume a spherical source[8] of radius R (that is $V = \frac{4}{3}\pi R^3$), homogeneously filled with a tangled field of average (transverse) strength $\langle B\rangle$. The constants $\nu_0 = 1.254 \times 10^{19}$ Hz, $c_\kappa(1.72) = 3.96 \times 10^{-42}$, and $c_\epsilon(1.72) = 2.08 \times 10^{-28}$ are taken from Pacholczyk (1970), and converted into our units, where necessary (note: 0.1 mT = 1 G). If we parameterize the source radius R in units of the radius R_{43} derived from the VLBA measurement this yields:

$$\langle B\rangle = 46\,\mu\mathrm{T}\times\delta^{-1}\left(\frac{R}{R_{43}}\right)^4, \quad (3)$$

and

$$n_{1000} = 3.54\times10^5\,\mathrm{m^{-3}}\times\delta^{-1}\left(\frac{R}{R_{43}}\right)^{4\alpha-7}. \quad (4)$$

The low apparent velocity and the jet/counter-jet ratio $\mathcal{R}_{\rm jc} = 4\ldots8$ of the parsec-scale jet (Tingay et al. 1998) argue for Doppler factors between $\delta = 1.2$ (for $\beta = 0.5, \theta = 55°$) and $\delta = 0.6$ ($\beta = 0.9, \theta = 70°$). However, it should be noted that the estimate of $\langle B\rangle$ from the self-absorption frequency ν_1 depends very strongly on both ν_1 ($\propto\nu_1^{2\alpha-5}$) and the source size ($\propto R^4$). It is, therefore, no more than an order of magnitude estimate. Nevertheless, we use the field strength (3) to convert observed characteristic frequencies $\nu_1^{\rm obs}$, $\nu_{\rm c}^{\rm obs}$ into electron energies:

$$\gamma_{\rm c} = (\nu_{\rm c}\delta^{-1}/4.2\times10^4\ \mathrm{Hz})^{1/2}(\langle B\rangle/1\,\mu\mathrm{T})^{-1/2} = 6400\,(R/R_{43})^{-2},$$

and

$$\gamma(\nu_1) = 153\,(R/R_{43})^{-2}.$$

Additionally, the energy density of the magnetic field within the source can be estimated:

$$u_B = 1.0\times10^{-3}\,\delta^{-2}(R/R_{43})^8\ \mathrm{J\,m^{-3}},$$

which obviously depends very steeply on the assumed source radius $R \le R_{43}$. In any case u_B is much higher than the radiation energy density of the CMB or the starlight in the core of Cen A. As the synchrotron luminosity $P_{\rm syn} = \delta^{\alpha-2}\int_{\nu_1}^{\frac{1}{2}\nu_{\rm c}} P_\nu \mathrm{d}\nu$ is well determined by our observations, we find a synchrotron radiation energy density:

$$u_{\rm syn} = \frac{P_{\rm syn}}{4\pi R_{43}^2 c} = 7.44\times10^{-4}\,\delta^{\alpha-2}(R/R_{43})^{-2}\ \mathrm{J\,m^{-3}}.$$

For $\delta \simeq 1$ and $R = R_{43}$ we get $u_{\rm syn} \lesssim u_B$. On the other hand, Centaurus A has been detected in γ-rays (Thompson et al. 1995; Steinle et al. 1998), showing a broad luminosity peak at $\nu_{\rm IC} = 3\times10^{19}$ Hz with $\nu F_\nu = 5\times10^{-13}\,\mathrm{W\,m^{-2}} = 5\times10^{13}$ Hz Jy, that is ~3 times more powerful then the synchrotron peak in Fig. 6. As we found electron energies $\langle\gamma\rangle$ of a few hundred (depending on R/R_{43}), which could up-scatter synchrotron photons from $\nu_{\rm syn} \simeq 3\times10^{13}$ Hz to $\nu_{\rm IC} = 2\gamma^2\nu_{\rm syn} \gtrsim 10^{19}$ Hz, it seems plausible to follow the standard interpretation of this second peak as *synchrotron self Compton* radiation (SSC, Jones et al. 1974; Chiaberge et al. 2001). The observed SSC luminosity $P_{\rm IC}$ requires

$$\frac{u_{\rm syn}}{u_B} = 0.744\,\delta^\alpha\left(\frac{R}{R_{43}}\right)^{-10} = \frac{P_{\rm IC}}{P_{\rm syn}} \gtrsim 3. \quad (5)$$

[8] In the absence of any structural information and in the view of the observational uncertainties in size and self-absorption frequency, this over-simplification seems appropriate.

Table 3. Intrinsic parameters of the synchrotron core in Centaurus A. Numerical values are given for Doppler factor $\delta = 1$ and a core radius $R_c = 1.26 \times 10^{14}$ m.

Parameter			Value	Units
Optically thin spectral index	α	$F_\nu \sim \nu^\alpha$	-0.36 ± 0.01	
Self-absorption frequency	ν_1	$=\nu(\tau = 1)$	$(4.5 \pm 0.5) \times 10^{10}$	Hz
Cutoff frequency	ν_c		8.0×10^{13}	Hz
Black hole mass	M_{bh}		6×10^7	$M_\odot$
Schwarzschild radius	R_S		1.8×10^{11}	m
Observed half-size at 43 GHz	R_{43}		$(1.5 \pm 0.3) \times 10^{14}$	m
Radius of synchrotron core	R_c		1.26×10^{14}	m
Doppler factor	δ	$\sqrt{1-\beta^2}/(1-\beta\cos\theta)$	1	
that is for $\theta = 50°$:				
Velocity	$\beta_{jet} = v_{jet}/c$		0.91	
Doppler factor at $\theta = 0$	δ_0		4.6	
that is for $\theta = 70°$:				
Velocity	$\beta_{jet} = v_{jet}/c$		0.61	
Doppler factor at $\theta = 0$	δ_0		2.0	
Magnetic field strength	$\langle B \rangle$	$\propto \delta^{-1} R_c^4$	26	μT
Relativistic particle density	n_{1000}	$\propto \delta^{-1} R_c^{4\alpha-7}$	3.73×10^5	m^{-3}
Minimum particle energy	$\gamma_{min} < \gamma(\nu_1)$	$\propto R_c^{-2}$	<204	$m_e c^2$
Cutoff particle energy	γ_c	$\propto R_c^{-2}$	8500	$m_e c^2$
Field energy density	u_B	$\propto \delta^{-2} R_c^8$	0.32×10^{-3}	J m^{-3}
Particle energy density	$u_{e\pm}$	$\propto \delta^{-2} R_c^{4\alpha-7}$	0.24×10^{-3}	J m^{-3}
Radiation energy density	u_{syn}	$\propto \delta^{\alpha-2} R_c^{-2}$	0.98×10^{-3}	J m^{-3}
Synchrotron luminosity	P_{syn}	$\propto \delta^{\alpha-2}$	6.8×10^{34}	W
Acceleration time scale	$\tau_{acc}(\gamma_c)$		4.0	days

Obviously, condition (5) is fulfilled if the radius of the synchrotron core, R_c, is slightly smaller than the observed value at 43 GHz: $R_c = 0.87\,R_{43} = 1.26 \times 10^{14}$m, that is well within the 20% error estimated for R_{43}. As observationally u_{syn} is much better determined than u_B, we will use the parameters of the synchrotron core derived from (5) in the following. They are summarized in Table 3. The here derived parameters of the synchrotron source are in good qualitative agreement with those derived by Chiaberge et al. (2001) on the basis of their SSC model assuming standard variability arguments and thus demonstrate that the basic properties of the synchrotron core do not rely too much on our detailed assumptions. However, it should be noted that the extension of the γ-ray peak into the X-ray region ($5 \times 10^{17} \ldots 2 \times 10^{18}$ Hz) is significantly steeper, $\nu^{-0.7}$ (Evans et al. 2004), than that expected from a *pure* SSC model. Thus an additional source of X-rays might be present (cf. Sect. 4.3).

4.1.2. Relation to the radio jet

To investigate the nature of the synchrotron source more closely, it is worthwhile to pursue the consequences of our essential measurements – namely the exact values of the cutoff frequency ν_c and the power-law slope α – even further: the most natural explanation for the high frequency cutoff is, that at the corresponding particle energy γ_c the radiation loss time $\tau_{loss}(\gamma_c)$ exactly equals the acceleration time scale $\tau_{acc}(\gamma_c)$:

$$\tau_{acc}(\gamma_c) \equiv \frac{\gamma_c}{d\gamma/dt} = \tau_{loss} = 3.8 \times 10^6\,\mathrm{s}\left(\frac{u_B+u_{syn}}{1\,\mathrm{J\,m^{-3}}}\right)^{-1} \gamma_c^{-1}$$
$$= 3.44 \times 10^5\,\mathrm{s} = 4.0\,\mathrm{days},$$

where we used u_B, u_{syn}, and γ_c from Table 3. The first thing to notice is, that $\tau_{acc} = 4$ days agrees well with the variability time scale $\tau_{var} \simeq 1$ day observed in the 100 MeV range (Kinzer et al. 1995). Second, $c\tau_{acc}(\gamma_c) = 1.03 \times 10^{14}$ m, is of the same order as the source radius R_c. Assuming an energy-independent τ_{acc} particles have to travel at least a distance $l_{acc} \simeq \log_2(\gamma_c/200) c\tau_{acc}(\gamma_c) = 5.5 \times 10^{14}$ m to be accelerated from $\gamma = 200$ to $\gamma = \gamma_c$. As $l_{acc} \gtrsim 4R_c$, the particles have to cross the source several times or gain a considerable amount of their energy on the way to the source.

This leads to the question of the nature of the synchrotron source and its distance from the central black hole. The most likely interpretation is, that the source represents the "base" of the radio jet, that is the innermost point at which electrons reach highly relativistic energies. From the width of the VLBA jet (Fig. 7) it seems that the jet is expanding freely out to a distance

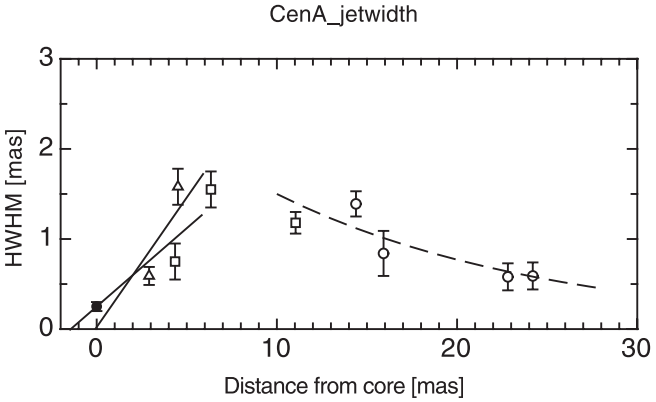

Fig. 7. Half width of the VLBA jet as a function of the distance from the radio core (•). The values have been derived from clearly resolved components C1 (○), C2 (□), and C3 (△) on the 8.4 GHz maps from Tingay et al. (1998). Two alternatives for the jet opening angle are shown: either the radio "core" represents the innermost (stationary) knot of the radio jet some ~1.4 mas (0.026 pc) from the origin (solid line, half opening angle 10°) or it is located at the core proper (dashed line, maximum opening angle 16°). Our measurements have been confirmed recently by Horiuchi et al. (2006).

of about 5 mas (=0.1 pc = 3×10^{15} m) from the VLBA core. In this region the jet half opening angle is between 10° and 16°. This leads to an upper limit of $d \leq 0.026\,\mathrm{pc} \simeq 6\,R_\mathrm{c}$ for the distance of the synchrotron source from the core proper.

The slope of the synchrotron powerlaw $\alpha = -0.36$ corresponds to an electron spectrum $n(\gamma) \propto \gamma^{-q}$ with $q = 1.72$. This is considerably flatter than the standard value expected from Fermi acceleration at a strong, non-relativistic shock ($q = 2$). However, it has been demonstrated by various authors (Kirk & Schneider 1987; Kirk & Heavens 1989) that first order Fermi acceleration at (oblique) relativistic shocks could produce power-law slopes between $q = 1.6$ and $q = 2$. An alternative way to produce such flat electron spectra could be provided by relativistic current sheets (Kirk 2005). In this context, it is instructive to check whether the magnetic field and relativistic particle energy density are close to equipartition ($u_B \simeq u_{\mathrm{e}\pm}$) as it seems to be the case in the terminal shocks (hot spots) of extended radio jets (Meisenheimer et al. 1989). With the parameters in Table 3 we find for the energy in electrons and positrons:

$$u_{\mathrm{e}\pm} = 1000\, m_\mathrm{e} c^2 n_{1000} \int_{0.1}^{8.5} g^{1-q} \mathrm{d}g = 2.4 \times 10^{-4}\, \delta^{-2} R_\mathrm{c}^{4\alpha-7}\,\mathrm{J\,m^{-3}}$$
$$\simeq 0.74 \times u_B,$$

where $g \equiv \gamma/1000$ and we assume $\gamma_\mathrm{min} = 100$. So, unless a lot more energy is stored in relativistic protons, the synchrotron core does not deviate far from equipartition.

To summarize, we interpret the synchrotron "core" of Centaurus A as the innermost point of its relativistic outflow, at which interaction with the surrounding medium leads to the onset of efficient particle acceleration within the jet flow. At our present knowledge, it cannot be decided whether this "visible base" of the jet is marked by an internal shock or magnetic reconnection phenomena in the relativistic flow. In any case, it seems likely that the onset of radiation from the jet is connected to deceleration of the flow to $\Gamma_\mathrm{jet} \lesssim 2.5$. As relativistic particles of moderate energies ($\gamma < 1000$) suffer smaller synchrotron losses, one might speculate that they are advected downstream with the jet flow, thus providing the "seed particles" which are required for efficient shock acceleration in the parsec-scale radio jet.

It is worth to note that recent observations of the kiloparsec jet with the Spitzer Space Telescope (Quillen et al. 2006; Brookes et al. 2006) have established that its synchrotron spectrum shows a radio-to-infrared power-law with $\alpha = -0.72$ which extends at least to $\nu = 10^{14}$ Hz. Assuming an equipartition magnetic field of ≃3 nT one derives that electrons in the kiloparsec jet have to be accelerated to energies $\gamma_\mathrm{max} \gtrsim 10^6$ (i.e. $100 \times \gamma_\mathrm{c}$ of the synchrotron core). This might indicate that the maximum energy scales with the size of the acceleration region.

4.2. Circum-nuclear dust emission from the parsec disk

As pointed out in Sect. 2 our current – very limited – coverage of the *uv*-plane leads us to the conclusion, that the center of Centaurus A is essentially unresolved along PA ≃ 40° but shows a clear indication for an extended component along PA ≃ 120°. Until future interferometric observations with other baselines allow us to constrain better the size and shape of the extended component, we simply assume that the visibility $V^{\mathrm{Feb.\ 28}}(\lambda) = 0.8\text{–}0.04(\lambda - 8\,\mu\mathrm{m})$ along PA = 108° ± 12° is caused by the superposition of the unresolved synchrotron core and a well resolved, inclined disk, the major axis of which must be orientated roughly perpendicular to PA = 37° ± 9°, along which we find $V(\lambda) \simeq 1$. The size of the disk is poorly confined by the present observations but needs to be ≳30 mas (=0.57 pc) at $\lambda = 13\,\mu$m, in order to be consistent with our simple two-component model. As there might be a marginal decrease in the visibility along PA ≃ 40° towards the longest wavelengths, only an upper limit of ∼12 mas can be given for the projected width of the disk. Figure 8 sketches this interpretation. Note that within the current uncertainties the major axis of the disk could well be orientated exactly perpendicular to the direction of the parsec scale radio jet at PA(jet) = 50° (Tingay et al. 1998) and could represent an inclined thin disk, the axis of which is aligned with the radio axis at 50° < θ < 70° with respect to our line-of-sight (cf. Table 3).

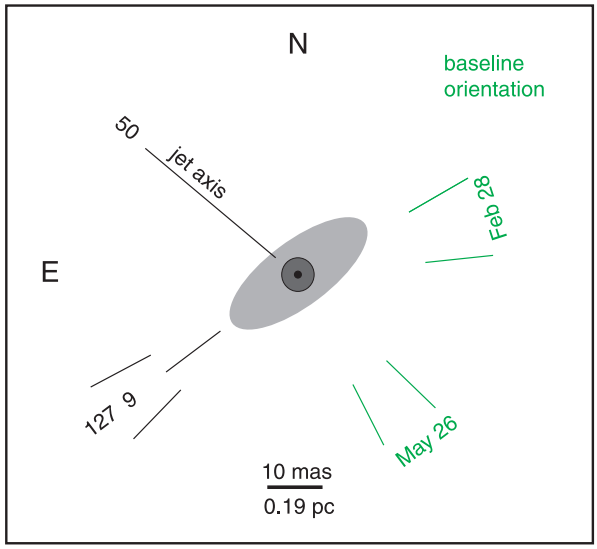

Fig. 8. Sketch of our model for the mid-infrared emission from the inner parsec of Centaurus A. We identify the unresolved point source of <6 mas *FWHM* (dark grey) with the VLBI core (*FWHM* = 0.5 ± 0.1 mas, indicated as black dot). It is surrounded by an elongated structure of dust emission (light grey) the major axis of which is orientated along PA = 127° ± 9° as inferred from the orthogonal baselines observed on May 26. From the visibilities observed with two baselines on February 28 we derive a major axis length of about 30 mas. Note that the major axis orientation is consistent with being perpendicular to the radio jet axis, and the axis ratio can be explained by a thin disk the axis of which is inclined by ∼66° with respect to our line-of-sight.

From the visibility $V^{\mathrm{Feb.\ 28}}(\lambda)$ and the extinction corrected flux values in Table 2 we derive $F_\mathrm{disk}(8.3\,\mu\mathrm{m}) = (0.21 \pm 0.10)$ Jy and $F_\mathrm{disk}(12.6\,\mu\mathrm{m}) = (0.71 \pm 0.20)$ Jy, respectively[9]. Interpreting this steep rise towards long wavelengths as the Wien tail of a blackbody spectrum from warm dust leads to a dust temperature of $T \simeq 240$ K. With this temperature we derive a rough estimate of the bolometric power emitted by the dust: $P_\mathrm{dust} \gtrsim 3 \times 10^{34}$ W. Since the dust disk seems too thin to cover more than 1π steradian (seen from the central accretion disk), we conclude, that a heating power $P_\mathrm{heat} \geq 10^{35}$ W is required to explain the apparent dust emission. As we will discuss in Sect. 4.3 the optical-UV power radiated by a nuclear accretion disk is insufficient to heat the dust. Thus other radiation sources must illuminate the dust disk. It seems that the most likely source for its heating is provided by X-ray radiation. Regarding the size of the dust disk,

[9] When assuming an unresolved core and a well resolved disk, F_disk is related to the core flux $F_{0,\nu}$ by $F_\mathrm{disk}(\lambda) = (\frac{1}{V(\lambda)} - 1)\, F_{\nu,0}(\lambda)$.

it is instructive to calculate the dust sublimation (inner) radius for the required heating power $P_{\rm heat} \gtrsim 10^{35}$ W and a sublimation temperature of 1500 K:

$$r_{\rm in} = 1.3\,{\rm pc}\left(\frac{P_{\rm heat}}{10^{39}\,{\rm W}}\right)^{1/2} \gtrsim 0.013\,{\rm pc}.$$

As this corresponds to <1 mas, that is <1/20 of our resolution, it is hard to determine how much the innermost parts of the dust disk could contaminate the flux from the unresolved core. In any case, we conclude, that the amount of dust emission from the central parsec of Centaurus A is most likely limited by the available illuminating radiation. Thus it is impossible to determine the gas and dust content of the innermost parsec from mid-infrared observations.

4.3. Thermal radiation from the core of Centaurus A

Even when allowing for the Doppler effect along the jet axis, the maximum photon energy $\delta_0 h\nu_{\rm c} < 1.5\,{\rm eV} \ll 13.6\,{\rm eV}$, of the synchrotron radiation from the core of Centaurus A cannot ionize hydrogen. Thus, the observation of narrow emission lines from the nucleus of Centaurus A requires a thermal ionization source. A crude upper limit for the ionizing flux from a thermal source (accretion disk?) within the core of Centaurus A might be obtained by assuming that the entire excess at $\lambda = 0.814\,\mu$m, $F_{\nu,0} - F_{\rm syn} \simeq 9$ mJy, is due to a thermal source[10] and that this source has an intrinsic spectrum resembling that of typical accretion disks in type 1 AGN, $F_\nu \sim \nu^{-0.6}$ out to $\nu = 6 \times 10^{16}$ Hz. This yields $P_{16} \simeq 3 \times 10^{34}$ W, that is only 0.1% of that of a typical Seyfert nucleus or $4 \times 10^{-5} \times L_{\rm Edd}$, the Eddington luminosity of the black hole. At such low luminosity (and correspondingly low accretion rate), the accretion flow onto the black hole will not occur via a thin accretion disk, but in the form of an Advection Dominated Accretion Flow (ADAF, Narayan & Yi 1995; Narayan et al. 1998). A further possibility to estimate the amount of thermal radiation can be based on the observed $\rm Br_\gamma$ flux of $6 \times 10^{-19}\,{\rm W\,m^{-2}}$ within a $3 \times 3\,\square''$ aperture (Neumayer et al., in prep.). Assuming, that the gas disk intercepts 0.7π steradian[11] of an isotropically emitted ionizing radiation and that every recombining H atom emits 0.004 Brγ photons on average (case A, Osterbrock 1989) one finds that $P_{\rm Lyc} = 1.3 \times 10^{34}$ W has to be emitted isotropically in the Lyman continuum. Thus, the above derived estimate for the thermal power, P_{16} seems sufficient to provide the ionizing flux which is needed to explain the observed line emission around the core of Centaurus A.

As outlined in Sect. 4.2, at least 10^{35} W of (isotropic) luminosity are required to account for the emission of the dust disk. Obviously this cannot be provided by the UV radiation of such a low luminosity accretion flow. Significantly more power is available in X-rays. So far, we have discussed the high frequency emission from the core of Centaurus A only in terms of the SSC model. Indeed, the low frequency tail of the inverse Compton (IC) radiation between 3×10^{15} and 10^{17} Hz, expected from the SSC models might provide some ionizing photons, which due to their hard spectrum could lead to rather high ionization states. As obvious from the δ_0 values in Table 3, we expect Doppler boosting of this IC radiation between a factor of 5 and 36 along the jet axis! In fact, recent observations with the adaptive optics spectrograph SINFONI reveal that coronal lines like [SiVI] are aligned along the jet axis (van der Werf et al. & Neumayer et al., in prep.). In addition, Chandra and XMM observations (Evans et al. 2004) between 2 and 7 keV ($\nu = 5$ to 17×10^{17} Hz) detected an absorbed ($N_{\rm H} \simeq 10^{23}\,{\rm cm^{-2}}$) continuum source with a $\nu^{-0.7}$ spectrum and a flux of $F_\nu = 63\,\mu$Jy at 1 keV ($2.42{\times}10^{17}$ Hz) which the authors interpret as emission from an accretion disk. As this spectrum is considerably steeper than that expected for pure SSC emission of the synchrotron core ($\nu^{-0.36}$), one needs to consider that part of the X-ray flux is of thermal origin: we obtain a rough estimate of the thermal contribution by integrating the $\nu^{-0.7}$ power-law between 10^{17} and 10^{19} Hz and subtracting the SSC contribution. This yields a thermal X-ray luminosity of $P_{\rm X,th} \gtrsim 1 \times 10^{35}$ W. To summarize, we conclude that the X-ray luminosity seems to be *just* able to heat the dust. Including the X-ray flux the thermal luminosity of the nucleus in Centaurus A is $P_{\rm th} \simeq 1.5 \times 10^{-4} \times L_{\rm Edd}$.

It should be mentioned that the high HI column would argue for $A_{\rm V} \simeq 50$ mag if the standard interstellar conversion $A_{\rm V}/N_{\rm H} = 5 \times 10^{-22}$ mag cm^2 would be assumed. Although this seems in conflict with our value $A_{\rm V} \simeq 14$ mag, one should note that for $A_{\rm V} = 14$ mag the ratio $A_{\rm V}/N_{\rm H} = 1.4 \times 10^{-22}$ mag cm^2 lies well in the range that has been found in other FR I radio galaxies (Balmaverde et al. 2006).

4.4. Comparison with other radio sources

We now compare our findings on Centaurus A with other AGN which host a similarly massive black hole. It is evident, that even the closest and least luminous Seyfert 2 galaxies (Circinus, NGC 1068) contain nuclear dust concentrations ("tori") which radiate 10 . . . 100× more powerful in the mid-IR than Centaurus A. As discussed in Sect. 4.2 this mainly might be explained by the lack of a heating source, while the total amount of cold dust in the inner parsecs can hardly be constrained. So certainly, Centaurus A is not a "well hidden" Seyfert galaxy.

Instead, it shares many properties of nearby FR I radio galaxies: morphology and luminosity of its parsec to kiloparsec jets is well in the range observed for nearby FR Is. As in other FR I galaxies (Balmaverde et al. 2006; Evans et al. 2006), its nuclear X-ray emission is produced at least partly at the base of the radio jet. Most of the dust extinction towards the core occurs in dust structures on scales of 50 to thousands of parsec. However, the existence of a narrow-line region which exhibits high ionization lines and our new evidence for a very compact nuclear dust disk (0.6 pc diameter) are features of Centaurus A, which are untypical for FR I radio galaxies. It is worth noting, that the small dust luminosity of Centaurus A places it among the "mid-IR weak" radio galaxies which comprise about half of a sample of FR II galaxies observed by Ogle et al. (2006) with the Spitzer Space Observatory.

The most unique feature of Centaurus A is its rather powerful synchrotron core, the spectrum of which peaks around 10^{14} Hz. Even the much more powerful radio galaxy M 87 which hosts a 50 times more massive black hole cannot compete with Centaurus A in this respect. Since relativistic beaming cannot account for the difference[12], we would like to argue that the luminous synchrotron core is an intrinsic property of Centaurus A.

[10] Note: the extremely faint "core" observed at $\lambda = 0.55\,\mu$m by Marconi et al. (2000), when corrected for $A_{\rm V} = 14$ mag, would have an intrinsic flux of $F_{\nu,0} \simeq 36$ mJy, much higher than any reasonable accretion disk spectrum could account for. We conclude therefore, that this flux does not come from the core proper.

[11] That is an angular range of ±10° or a full disk height of 7 pc at half the radius of the disk, $r/2 = 20$ pc.

[12] Most authors believe that the M 87 jet is within about 20° of our line of sight. This would argue for a significantly higher Doppler factor ($\delta \gg 1$) in M 87 than inferred for Centaurus A.

It is attractive to speculate, that the more-than-average amount of dust and gas in the innermost parsec, as established by our detection of extended mid-infrared emission, could play an important role in building up the strong internal shock at $d < 0.026$ pc which is capable of converting a significant fraction of the outflowing kinetic energy into relativistic particles already such close to the core.

Finally, we would like to discuss the term "mis-directed" BL Lac which has been used by several authors to explain the unique properties of the non-thermal core in Centaurus A. In the framework of the unified scheme (Urry & Padovani 1995) any FR I radio galaxy qualifies as "mis-directed BL Lac". The question is, however, whether the *special properties* of the synchrotron core in Centaurus A are typical for BL Lac objects. The strongest argument against this is the bulk Lorentz factor $\Gamma_{\rm jet} < 2.5$, which seems outside the range $5 < \Gamma_{\rm jet} < 32$ derived by Urry & Padovani (1995) for radio-selected BL Lac objects. Accordingly, neither the fact that the synchrotron spectrum reaches to frequencies as high as 10^{14} Hz, nor the γ-ray emission, nor the variability time scale seem to be caused by relativistic beaming (we derive a Doppler factor $\delta \simeq 1$). Rather they seem to be a consequence of violent interaction between the relativistic outflow and the surrounding medium, which occurs much closer to the central black hole (at $r < 10^4\,R_{\rm S}$) than in typical FR I radio galaxies. However, we cannot exclude, that the parsec jet of Centaurus A contains a relativistic ($\Gamma > 5$) "spine", which leaves no imprint on any of the observations obtained so far.

5. Conclusions

Our interferometric observations of Centaurus A in the *N*-band ($8 < \lambda < 13\,\mu$m) provide strong evidence that its mid-infrared emission is dominated by an unresolved synchrotron core. The size of this core is most likely given by the size of $R_{43} \simeq 0.01$ pc, derived from VLBI observations at 43 GHz. Additionally, the observations with interferometric baselines orientated roughly perpendicular to the parsec scale radio jet revealed an extended component which naturally can be interpreted as a geometrically thin, dusty disk, the axis of which coincides with the radio jet. Its diameter is about 0.6 pc. It contributes between 20% (at short wavelengths, $\lambda \simeq 8\,\mu$m) and 40% (at $\lambda \simeq 13\,\mu$m) to the nuclear flux from Centaurus A and contains dust which is heated up to about 240 K.

We demonstrate, that assuming an extinction $A_{\rm V} = (14 \pm 2)$ mag, all flux measurements of the core between radio and near infrared frequencies can be fitted nicely by a synchrotron spectrum, although there is evidence for variability. The spectrum is characterized by a rather flat power-law $F_\nu \sim \nu^{-0.36}$ which cuts off above $\nu_{\rm c} = 8 \times 10^{13}$ Hz and becomes optically thick below $\nu_1 \simeq 4.5 \times 10^{10}$ Hz. Following the usual interpretation of the γ-ray emission from Centaurus A as Synchrotron Self Compton (SSC) radiation we derive a magnetic field strength of 26 μT and an maximum energy of relativistic electrons of $\gamma_{\rm c} = E_{\rm c}/m_{\rm e}c^2 = 8500$. With these parameters we derive an acceleration time scale of $\tau_{\rm acc} = 4$ days, which is in good agreement with the fastest flux variations, observed at X-ray frequencies. We point out, however, that the spectral slope at X-ray frequencies does not fit into the SSC model, but requires an additional X-ray emission process.

Our SSC model argues for a Doppler factor $\delta \simeq 1$ which – together with the jet-counter jet ratio of the radio jets on parsec scale – results in an upper limit $\Gamma_{\rm jet} < 2.5$. Such a low bulk Lorentz factor does not fit to the concept of a "mis-directed BL Lac object", unless there exists a highly relativistic "spine", which has no observable signature.

Finally, we try to estimate the thermal luminosity from the accretion flow around the black hole in Centaurus A: taking the observed excess at $\lambda < 1\,\mu$m above the synchrotron spectrum as signature of a thermal core component and assuming that part of the X-ray flux is of thermal origin, we find a thermal power $P_{\rm th} \simeq 1.3 \times 10^{35}$ W $\simeq 1.5 \times 10^{-4} \times L_{\rm Edd}$. Although this is at least two orders of magnitude below the value in highly radiation-efficient accreting AGN (e.g. Seyfert galaxies), it is still substantially higher than the values which are typical for FR I radio galaxies. Nevertheless, it remains in the range predicted for Advection Dominated Accretion Flows (ADAF, Narayan et al. 1998) where most of the accretion energy is lost unseen or is channeled into kinetic jet power. At the present state of knowledge, one cannot decide whether its relatively high thermal luminosity indicates that Centaurus A currently is undergoing a transition between low and high radiative efficiency (cf. Falcke et al. 2004) or whether this intermediate state can be maintained over long periods of time. In any case, the special properties of Centaurus A – the closest and best resolved active galactic nucleus – seem to provide a counter-example against simple unified schemes, which try to explain FR I radio galaxies and BL Lacertae objects by orientation effects alone.

Acknowledgements. We thank Paul van der Werf for access to the SINFONI data before publication. Several aspects of the paper could be clarified in discussions with John Kirk and Max Camenzind. We are particularly grateful to the referee, Yuan Feng, whose constructive criticism helped us clarify and improve this paper substantially.

References

Arsenault, R., Alonso, J., Bonnet, H., et al. 2003, in Adaptive Optical System Technologies II, ed. P. L. Wizinowich, & D. Bonaccini, Proc. SPIE, 4839, 174
Baade, W., & Minkowski, R. 1954, ApJ, 119, 215
Bailey, J., Sparks, W. B., Hough, J. H., & Axon, D. J. 1986, Nature, 322, 150
Balmaverde, B., Capetti, A., & Grandi, P. 2006, A&A, 451, 35
Bolton, J. G., Stanley, G. J., & Slee, O. B. 1949, Nature, 164, 101
Bregman, J. N. 1990, A&A Rev., 2, 125
Brookes, M. H., Lawrence, C. R., Keene, J., et al. 2006, ApJ, 646, L41
Chiaberge, M., Capetti, A., & Celotti, A. 2001, MNRAS, 324, L33
Clarke, D. A., Burns, J. O., & Norman, M. L. 1992, ApJ, 395, 444
Cutri, R. M., Skrutskie, M. F., van Dyk, S., et al. 2003, 2MASS All Sky Catalog of point sources (The IRSA 2MASS All-Sky Point Source Catalog, NASA/IPAC Infrared Science Archive `http://irsa.ipac.caltech.edu/applications/Gator/`)
Döbereiner, S., Junkes, N., Wagner, S. J., et al. 1996, ApJ, 470, L15
Evans, D. A., Kraft, R. P., Worrall, D. M., et al. 2004, ApJ, 612, 786
Evans, D. A., Worrall, D. M., Hardcastle, M. J., Kraft, R. P., & Birkinshaw, M. 2006, ApJ, 642, 96
Falcke, H., Körding, E., & Markoff, S. 2004, A&A, 414, 895
Hardcastle, M. J., Worrall, D. M., Kraft, R. P., et al. 2003, ApJ, 593, 169
Häring-Neumayer, N., Cappellari, M., Rix, H.-W., et al. 2006, ApJ, 643, 226
Hawarden, T. G., Sandell, G., Matthews, H. E., et al. 1993, MNRAS, 260, 844
Horiuchi, S., Meier, D. L., Preston, R. A., & Tingay, S. J. 2006, PASJ, 58, 211
Israel, F. P. 1998, A&ARv, 8, 237
Jaffe, W. J. 2004, in New Frontiers in Stellar Interferometry, Proc. SPIE, 5491, Bellingham, WA: The International Society for Optical Engineering, ed. W. A. Traub, 715
Jaffe, W., Meisenheimer, K., Röttgering, H. J. A., et al. 2004, Nature, 429, 47
Jones, T. W., O'dell, S. L., & Stein, W. A. 1974, ApJ, 188, 353
Junkes, N., Haynes, R. F., Harnett, J. I., & Jauncey, D. L. 1993, A&A, 269, 29
Kellermann, K. I., Zensus, J. A., & Cohen, M. H. 1997, ApJ, 475, L93
Kemper, F., Vriend, W. J., & Tielens, A. G. G. M. 2004, ApJ, 609, 826
Kinzer, R. L., Johnson, W. N., Dermer, C. D., et al. 1995, ApJ, 449, 105
Kirk, J. G. 2005, ArXiv Astrophysics e-prints

Kirk, J. G., & Heavens, A. F. 1989, MNRAS, 239, 995
Kirk, J. G., & Schneider, P. 1987, ApJ, 315, 425
Leinert, C., Graser, U., Przygodda, F., et al. 2003, Ap&SS, 286, 73
Lenzen, R., Hofmann, R., Bizenberger, P., & Tusche, A. 1998, in Infrared Astronomical Instrumentation, ed. A. M. Fowler, Proc. SPIE, 3354, 606
Lepine, J. R. D., Braz, M. A., & Epchtein, N. 1984, A&A, 131, 72
Macomb, D. J., Akerlof, C. W., Aller, H. D., et al. 1995, ApJ, 449, L99
Marconi, A., Schreier, E. J., Koekemoer, A., et al. 2000, ApJ, 528, 276
Meisenheimer, K., Roser, H.-J., Hiltner, P. R., et al. 1989, A&A, 219, 63
Morel, S., Ballester, P., Bauvir, B., et al. 2004, in New Frontiers in Stellar Interferometry, Bellingham, WA: The International Society for Optical Engineering, ed. W. A. Traub, Proc. SPIE, 5491, 1666
Narayan, R., & Yi, I. 1995, ApJ, 452, 710
Narayan, R., Mahadevan, R., & Quataert, E. 1998, in Theory of Black Hole Accretion Disks, ed. M. A. Abramowicz, G. Bjornsson, & J. E. Pringle, 148
Ogle, P., Whysong, D., & Antonucci, R. 2006, ApJ, 647, 161
Osterbrock, D. E. 1989, Astrophysics of gaseous nebulae and active galactic nuclei (Research supported by the University of California, John Simon Guggenheim Memorial Foundation, University of Minnesota, et al. Mill Valley, CA, University Science Books), 422
Pacholczyk, A. G. 1970, Radio astrophysics. Nonthermal processes in galactic and extragalactic sources, Series of Books in Astronomy and Astrophysics (San Francisco: Freeman)
Quillen, A. C., Brookes, M. H., Keene, J., et al. 2006, ApJ, 645, 1092
Ratzka, T., Chesneau, O., Meisenheimer, K., & Tristram, K. 2006, in Advances in Stellar Interferometry, ed. J. D. Monnier, M. Schöller, & W. C. Danchi, Proc. SPIE, 6268
Rejkuba, M. 2004, A&A, 413, 903
Rothschild, R. E., Band, D. L., Blanco, P. R., et al. 1999, ApJ, 510, 651
Rousset, G., Lacombe, F., Puget, P., et al. 1998, in Adaptive Optical System Technologies, ed. D. Bonaccini, & R. K. Tyson, Proc. SPIE, 3353, 508
Schartmann, M., Meisenheimer, K., Camenzind, M., Wolf, S., & Henning, T. 2005, A&A, 437, 861
Schreier, E. J., Marconi, A., Axon, D. J., et al. 1998, ApJ, 499, L143
Steinle, H., Bennett, K., Bloemen, H., et al. 1998, A&A, 330, 97
Thompson, D. J., Bertsch, D. L., Dingus, B. L., et al. 1995, ApJS, 101, 259
Tingay, S. J., Jauncey, D. L., Reynolds, J. E., et al. 1998, AJ, 115, 960
Tristram, K., Meisenheimer, K., Jaffe, W., et al. 2006, A&A, in preparation
Turner, P. C., Forrest, W. J., Pipher, J. L., & Shure, M. A. 1992, ApJ, 393, 648
Urry, C. M., & Padovani, P. 1995, PASP, 107, 803